行政院國家科學委員會專題研究計畫 成果報告

大氣陸地交互機制的純量來源強度研究(2/2)
研究成果報告(完整版)

計 畫 類 別 ：個別型
計 畫 編 號 ：NSC 95-2111-M-002-005-
執 行 期 間 ：95 年 08 月 01 日至 96 年 07 月 31 日
執 行 單 位 ：國立臺灣大學生物環境系統工程學系暨研究所

計 畫 主 持 人：謝正義

計畫參與人員：碩士班研究生-兼任助理：賴玫君、黃丞瑋

處 理 方 式 ：本計畫可公開查詢

中 華 民 國 96 年 10 月 31 日

行政院國家科學委員會專題研究計畫成果報告

大氣陸地交互機制的純量來源強度研究

Scalar flux footprint analysis and modeling for land-atmosphere exchange

計畫編號：NSC 95-2111-M-002-005

執行期限：95 年 8 月 1 日至 96 年 7 月 31 日

主持人：謝正義 國立台灣大學 生物環境系統工程系

hsieh@ntu.edu.tw

計畫參與人員：賴玫君 黃丞瑋 台灣大學 生物環境系統工程所

Abstract

This study investigated a two-dimensional Lagrangian stochastic dispersion model for estimating water vapor fluxes and footprint over homogeneous and inhomogeneous surfaces. Over the homogeneous surface, particle trajectories were computed from a 2-D Lagrangian model forced by Eulerian velocity statistics determined by Monin-Obukhov similarity theory (MOST). For an inhomogeneous surface, the velocity and atmospheric stability profiles were computed using a second-order Eulerian closure model, and then these local profiles were used to drive the Lagrangian model. The model simulations were compared with water vapor flux measurements carried out above an irrigated bare soil site and an irrigated potato site. The inhomogeneity involved a step change in surface roughness, humidity, and temperature. Good agreement between eddy-correlation

measured and Lagrangian model predicted water vapor fluxes was found for a wide range of stability conditions. Hence, this analysis demonstrates the practical utility of second-order closure models in conjunction with Lagrangian analysis to estimate the scalar footprint in planar inhomogeneous flows.

1. Introduction

Developing explicit relationships between scalar sources and sinks at the surface and turbulent fluxes in the atmosphere is becoming a central research topic in biosphere-atmosphere exchange given the proliferation of the number of sites participating in FluxNet, a global network aimed at quantifying long-term carbon dioxide (CO_2) and water vapor (H_2O) fluxes using the eddy-covariance method (e.g., Baldocchi et al., 2001). In deriving prognostic relationship between the flux and source areas (or footprint), both analytical (Eulerian) models (e.g., Horst and Weil, 1994, 1992; Gash, 1986) and Lagrangian models (e.g., Flesch, 1996; Flesch et al., 1995, Leclerc and Thurtell, 1990) have been employed. Large eddy simulations (LES) of footprint have also been investigated with some success albeit for a restricted domain (Leclerc et al., 1997; Kljun et al., 2002, 2004). About a decade ago, Finn et al. (1996) concluded that analytical and Lagrangian models provide similar estimates of footprint distances in homogeneous flows. However, they indicated that the Lagrangian model has a broader range of applications (e.g., for variable source strength cases) when compared to the analytical model thus permitting wider range of field conditions to be incorporated (e.g.. Kaharabata et al., 1997; Schmid 2002; Marcolla and Cescatti 2005), which is desirable for a large number of FluxNet sites.

One difficulty in implementing the Lagrangian model for estimating the flux and footprint derives from the need to specify the velocity field and atmospheric stability effects, especially when the flow is not planar homogeneous (Schmid 2002). For a stationary and planar homogeneous flow field, these velocity profiles can be readily estimated from Monin-Obukhov similarity theory (MOST). For canopy flows or above a

non-homogeneous surface such as a general irrigated agricultural area where a step change in surface roughness, moisture, and temperature conditions exists, MOST is no longer applicable. Hence, the Lagrangian model in conjunction with MOST cannot be readily applied (Hsieh et al., 1997). To overcome this problem, Luhar and Rao (1994) used a second-order closure model (Rao et al., 1974) to first solve for the velocity and temperature fields, and then these flow fields were used to drive the Lagrangian model and estimate the flux and footprint. Luhar and Rao's (1994) approach is attractive since this method avoids the assumption of planar homogeneous flow conditions. Despite this progress, two important issues remain that require systematic investigations: (1) the Lagrangian model calculations of Luhar and Rao (1994) remain one-dimensional and do not consider the fluctuation part of the streamwise velocity, and (2) this linkage between the Lagrangian and higher-order Eulerian closure models still awaits systematic field testing across a range of inhomogeneity types.

In this study, the two-dimensional Lagrangian model is used to explore the scalar flux and footprint over homogeneous and inhomogeneous surfaces where the fluctuation part of the streamwise velocity is explicitly considered. Next, field-testing of the Lagrangian model above two inhomogeneous surfaces is conduced. The first test is an irrigated bare soil site where the source area for water vapor is well defined within a larger non-irrigated bare soil region (i.e. no change in momentum roughness). The second test is an irrigated potato field surrounded by a desert. Since the airflow from dry to wet cannot be treated as homogeneous, the Lagrangian model must be linked to a two-dimensional second-order closure model to estimate water vapor flux and footprint.

Discussions on the performance of the Lagrangian model along with comparisons with these field experiments are presented.

2. Methods

2.1 The Lagrangian stochastic dispersion model

The Lagrangian model is based on the assumption that the evolution of the particle position and velocity is a Markov process. The basic concepts, details, and many references can be found in Rodean's (1996) monograph. Following this assumption, the stochastic equations describing the particle velocity and position are

$$\begin{aligned} du_i &= a_i(x_i,u_i,t)dt + b_{ij}(x_i,u_i,t)d\lambda_j \\ u_i(t) &= u_i(t_0) + \int_{t_0}^{t} du_i \end{aligned}, \tag{1}$$

and

$$\begin{aligned} dx_i &= u_i dt \\ x_i(t) &= x_i(t_0) + \int_{t_0}^{t} dx_i \end{aligned}, \tag{2}$$

where the sub-indexes i and j = 1, 2, or 3 with summation implied over repeated indexes, and x_1 = x, x_2 = y, x_3 = z, and u_1 = u, u_2 = v, u_3 = w are the longitudinal, lateral, and vertical velocities, respectively (since two-dimensional cases are considered, i and j each take on values of 1 and 3). As is common in stochastic differential equations, *a* can be interpreted as a drift coefficient, *b* is the random acceleration coefficient, *dt* is the time interval, and $d\lambda$ is a Gaussian random increment with zero mean and variance *dt*. Once coefficients *a* and *b* are determined from the flow field, then the formulation for particle trajectories can be established. For determining *a*, Thomson's (1987) well-mixed

condition is used while *b* can be determined from Kolmogorov's Lagrangian theory for the inertial subrange. The well-mixed condition states that if the tracer particles are initially uniformly distributed (well-mixed), they should remain so at all times during the dispersion process. Unfortunately, the well-mixed condition is not sufficient for selecting a unique solution for the coefficient *a* when the flow is two- or three- dimensional. Efforts have been made to provide a criterion for distinguishing better Lagrangian stochastic formulations within the "well-mixed" family (e.g., Reynolds, 1998a, b; Borgas et al., 1997; Wilson and Flesch, 1997), but improvements over Thomson's (1987) model was rather mixed (Sawford, 1999; Kurbanmuradov and Sabelfeld, 2000). For this reason, the steady state solution of Thomson's model is adopted with coefficients *a* and *b* given by

$$a_i = -b_{ik} b_{jk} (V^{-1})_{jk} (u_k - U_k) + \frac{\phi_i}{g_a} \tag{3a}$$

$$\frac{\phi_i}{g_a} = \frac{1}{2}\frac{\partial V_{il}}{\partial x_l} + \frac{\partial U_i}{\partial t} + U_l \frac{\partial U_i}{\partial x_l} + \left(\frac{1}{2}(V^{-1})_{lj}\left(\frac{\partial V_{il}}{\partial t} + U_m \frac{\partial V_{il}}{\partial x_m}\right) + \frac{\partial U_i}{\partial x_j}\right)(u_j - U_j) + \frac{1}{2}(V^{-1})_{lj}\frac{\partial V_{il}}{\partial x_k}(u_j - U_j)(u_k - U_k), \tag{3b}$$

$$b_{ij} = \delta_{ij}(C_0\varepsilon)^{1/2} \approx \delta_{ij}\left(\frac{2\sigma_w^2}{t_L}\right)^{1/2}. \tag{4}$$

In (3a), (3b), and (4), the sub-indices i and j = 1, 2, and 3 with summation over the repeated index, U_i is the mean Eulerian velocity (U_1 = U is the mean streamwise velocity, U_2 = V is the mean lateral velocity, and U_3 = W is the mean vertical velocity), the tensor V_{ij} is defined as $V_{ij} = \overline{(u_i - U_i)(u_j - U_j)}$, the over bar denotes ensemble average, σ_w^2, vertical velocity variance, is the one-dimensional form of V_{ij}, C_0 is Lagrangian

Kolmogorov constant and ε is the mean turbulent kinetic energy dissipation rate, and the quantity $C_0\varepsilon$ is approximated by $2\sigma_w^2/t_L$, where t_L is the Lagrangian de-correlation time scale. The derivation of (3) to (4) can be found in Thomson (1987) and will not be repeated here. Using (1) to (4), trajectories of fluid particles can be computed and concomitant scalar fluxes and footprint can be obtained.

2.2 The velocity field

To drive the Lagrangian model, the first and second moments of the velocity field have to be determined a priori. For a stationary and planar homogeneous flow, these profiles can be expressed via MOST as

$$W(z) = 0 \tag{5}$$

$$U(z) = \frac{u_*}{k}\left[\ln\left(\frac{z-d}{z_o}\right) - \psi_m\right] \tag{6}$$

$$\sigma_w = 1.25u_*\left(1 - 3\frac{z-d}{L}\right)^{1/3} \tag{7}$$

where u_* is the friction velocity, z_o is the surface roughness, d, is the zero plane displacement, L is the Obukhov length, k (= 0.4) is von Karman constant, and ψ_m is the momentum stability correction function (Brutsaert, 1984). The difficulty for driving a two-dimensional Lagrangian model stems from the specification of σ_u (the standard deviation of U) profile since σ_u may not follow MOST scaling. Here, two profiles of σ_u are considered:

$$\sigma_u = 2.5u_*\left(1 - 3\frac{z-d}{L}\right)^{1/3} \tag{8}$$

$$\sigma_u = \left(0.35 w_*^2 + 2.0 u_*^2\right)^{1/2}; \qquad w_* = \left(-\frac{u_*^3 h_b}{Lk} \right)^{1/3} \tag{9}$$

In (8), σ_u is described as a function of *(z-d)/L* as suggested by Kader and Yaglom (1990) and Hsieh and Katul (1997). In (9), σ_u does not obey MOST and is a function of a convective velocity scale w_* and the boundary layer height, h_b (= 2,000 m, assumed in this study). The stability correction functions (ψ_m) for stable and unstable conditions and t_L profiles are described in the Appendix. The input parameters for this two-dimensional Lagrangian model are: u_*, z_o, d, L, and measurement height, z_m, where z_o and d can be approximated by 0.1h and 0.66h, respectively, and h is the canopy height.

For an inhomogeneous surface, where a step change in momentum and scalars occur, the velocity and atmospheric stability fields cannot be computed from MOST as the flow is no longer planar-homogeneous. Here, a second-order closure model is proposed instead of MOST. This model consists of:

1) three mean field equations for streamwise velocity (U), vertical velocity (W), and temperature (Θ).

$$U\frac{\partial U}{\partial x} + W\frac{\partial U}{\partial z} = -\frac{\partial \overline{uw}}{\partial z} \tag{10a}$$

$$\frac{\partial U}{\partial x} + \frac{\partial W}{\partial z} = 0 \tag{10b}$$

$$U\frac{\partial \Theta}{\partial x} + W\frac{\partial \Theta}{\partial z} = -\frac{\partial \overline{\theta w}}{\partial z} \tag{10c}$$

2) four Reynolds stress $(\overline{uu}, \overline{vv}, \overline{ww}, \overline{uw})$ equations for velocity variance and covariance.

$$U_j(\overline{u_i u_k})_{,j} + (\overline{u_j u_k})U_{i,j} + (\overline{u_j u_i})U_{k,j} - \frac{g}{T_o}(\overline{u_k\theta}\delta_{3i} + \overline{u_i\theta}\delta_{3k}) = -(\overline{u_i u_k u_j})_{,j} - (\overline{u_k p_{,j}} + \overline{u_i p_{,k}}) - 2\bar{\varepsilon}\frac{\delta_{ik}}{3} \quad (11)$$

where $i = k = 1$, 2, or 3, or $i = 1$ and $k = 3$, and $\bar{\varepsilon}$ is the dissipation rate of turbulent kinetic energy ($= \overline{u_i u_i}/2$).

3) one equation each for heat flux $(\overline{\theta w})$,

$$U_j(\overline{\theta u_i})_{,j} + (\overline{\theta u_j})U_{i,j} + (\overline{u_j u_i})\Theta_{,j} - \frac{g}{T_o}(\overline{\theta\theta}\delta_{3i}) = -(\overline{\theta u_i u_j})_{,j} - (\overline{\theta p_{,i}}) \quad (12)$$

where $i = 1$ or 3,

4) one equation for energy dissipation rate $(\bar{\varepsilon})$.

$$\bar{\varepsilon} = k_\varepsilon(\overline{u_i u_i})^{3/2}/k_L \quad (13)$$

where k_ε is a similarity constant and k_L is a mixing length scale. A review of several closure techniques can be found in Stull (1988) and are not repeated here. The closure formulations based on Wichmann and Schaller (1986) are adopted here. The methods for assigning boundary conditions are described in the Appendix.

2.3 Flux and footprint calculations

To calculate fluxes and footprints, scalar particles are released from the canopy height. For a horizontally homogeneous surface, calculations of flux and footprint only depend on the relative distance between the flux measurement point and the emission point, and the scalar flux, F, at the point (x, z) can be calculated using (Hsieh et al., 2000)

$$F(x,z) = \frac{S}{N}(n_\uparrow - n_\downarrow), \quad (14)$$

where S is the surface source strength (kg/m^2/s), $n_\uparrow$ and $n_\downarrow$ are the number of particles reaching height z at position x with upward and downward vertical velocities, respectively, and N is the total number of particles released. The footprint, f(x,z), can be calculated by differentiating the normalized flux (i.e., *F(x, z)/S*) with respect to x at (x, z) as

$$f(x,z) = \frac{\partial F(x,z)/S}{\partial x} \tag{15}$$

In essence, the footprint describes the relative contribution of each source element to the measured flux.

However, for an inhomogeneous surface, the flux and footprint calculations will also depend on the actual location of the emission point. In this case, flux estimation necessitates placement of a large number of upwind emission points along a line source and compute the following:

$$C(x,z) = \int_0^x \int_{-\infty}^{\infty} S(x_0) P(x,z,t \mid x_0, z_0, t_0) dt_0 dx_0 \tag{16}$$

$$F(x,z) = w(x,z) C(x,z) \tag{17}$$

where C is the mean scalar concentration and P is the transition probability density function (m^{-2}) that describes the probability density of a tracer particle originally released at (x_0, z_0, t_0) to be found at (x, z, t). Suppose the line source is divided into n segments, each having a uniform source density S_j over its width, Δx_j, where j = 1, ..., n. Equations (16) and (17) can be combined together and the flux at the measurement point (x_m, z_m) can be calculated as

$$F(x_m, z_m) = \sum_{j=1}^{n} \Delta x_j S_j(x_j) \frac{M_j^{\uparrow}(x_m + \Delta x, z_m)}{\Delta x} - \Delta x_j S_j(x_j) \frac{M_j^{\downarrow}(x_m + \Delta x, z_m)}{\Delta x} \tag{18}$$

where $M_j^{\uparrow}(x_m+\Delta x, z_m)$ and $M_j^{\downarrow}(x_m+\Delta x, z_m)$ are the probability of particles from source S_j passing the location between (x_m, z_m) and $(x_m+\Delta x, z_m)$ with positive and negative vertical velocities, respectively. Figure 1 illustrates the particle release methodology for inhomogeneous conditions.

3. Experiments

Two experimental data sets were used to test the Lagrangian model for inhomogeneous conditions. The first experiment was carried out above an irrigated bare soil site, where the Lagrangian model was tested against the measured water vapor flux (LE) at a fixed point. The second experiment was performed above an irrigated potato site, where the Lagrangian model was tested against water vapor flux measurements conducted along a progression of distances downwind from a transition (Baldocchi and Rao, 1995).

For homogeneous conditions, data collected above 1) a sagebrush canopy (z_o = 0.14 m, h = 0.75 m) described in Leclerc et al. (1997) and 2) a peach orchard canopy ($z_o \approx$ 0.4 to 0.54 m, h ≈ 3.1 to 4.2 m, d ≈ 2.1 to 2.8 m) described in Leclerc et al. (2003) are employed.

3.1 Bare soil site

This experiment was performed above a uniformly irrigated bare soil patch within a large dry soil field at the Campbell tract facility at the University of California in Davis. The Campbell tract facility is a 500 m by 500 m bare soil site (z_o = 1.7 mm, determined from the mean wind profile as described in Hsieh et al., 1997). The site is equipped with

a sprinkler irrigation system capable of irrigating a 120 m by 110 m soil patch with uniformity coefficients of about 85% (see Katul and Parlange, 1992; Parlange et al., 1992 for details on the irrigation system). The irrigation was carried out on the evening of August 21, 1993, and only data collected after the irrigation were used. The edge of the irrigated boundary from the tower varied from 80 m to 100 m depending on the wind direction. Two eddy-correlation systems, each consisting of a CA27 one-dimensional sonic anemometer and a Krypton hygrometer, were used to measure the vertical velocity and water vapor fluxes at 1.12 m and 2.9 m above the ground surface. The water vapor fluxes measured at 2.9 m were utilized as a reference and water vapor flux measurements at 1.12 m were used to test the Lagrangian model predictive skills. A Gill tri-axial sonic anemometer positioned at 1.96 m from the surface was used to measure the wind velocity statistics and sensible heat flux (H). The sampling frequency was 21 Hz and the sampling period was 26 minutes, resulting in 32,768 data points from each measured flow variable. The longitudinal velocity was rotated along the mean wind direction so that V, the mean lateral velocity, was zero for each run. A unique feature about this experiment is that the water vapor source area is well defined.

3.2 Potato site

A brief description of this experiment is presented below and the details can be found in Baldocchi and Rao (1995). The experimental site was an irrigated potato field, which surrounded by a desert soil. The crop was irrigated every one to three days to ensure maximum productivity and limited water stress. The surface roughness height was 5 mm for the desert soil and 50 mm for the potato field. A stationary eddy-correlation

system was set at 800 m downwind from the transition and used to measure turbulent fluxes of momentum, sensible heat, latent heat, and CO_2 above the potato field. A mobile eddy-correlation system was used to measure these fluxes along a progression of distances, 1 m, 38.4 m, 72 m, 91 m, 136 m, and 295 m, downwind from the transition. Both systems were set at 4 m above the ground and all the data were normalized by the measurements from the stationary system. Based on the mean upwind meteorological conditions (0.35 m s^{-1} for friction velocity, 350 W m^{-2} for sensible heat flux, and 100 W m^{-2} for latent heat flux), the second order closure model was used to compute the flow field, which were then utilized to drive the Lagrangian model for estimating the variability in water vapor fluxes along the progression of downwind distances.

4. Results and Discussion

4.1 Model simulations under homogeneous condition

We compare the Lagrangian model results under homogeneous condition with field measurements before using these models for analyzing field measurements in planar inhomogeneous flows. Figure 2a shows a typical predicted relative flux at 10 m above the ground as a function of downwind distance (fetch) by the Lagrangian model and measurements (circles) under unstable conditions (L = -55 m, u_* = 0.4 m/s, z_o = 0.14 m, h = 0.75 m) over a homogeneous sagebrush canopy described in Leclerc et al. (1997). Figure 2b is the same as Figure 2a but for a stronger unstable condition (L = -32 m and u_* = 0.29 m/s). In Figures 2a and 2b, the solid line represents the Lagrangian model prediction with σ_u profile from (8) and the dash line represents simulation with σ_u profile from (9). Notice that both σ_u profiles result in similar footprint estimations. Hence, only

the model predictions with (9) are presented hereafter. Good agreement between measured and predicted fluxes was found in Figure 2. The relative fluxes as a function of fetch for neutral and stable (L = 100 m) conditions are also shown in Figure 3. The observation height, surface roughness, and friction velocity for Figure 3 are the same as Figure 2 though there were no flux measurements to compare with under stable and neutral conditions. As expected, the 90 percent flux fetch requirement varies significantly with variations in atmospheric stability, and this fetch requirement progressively gets longer for the same measurement height as the flow changes from unstable to neutral to stable conditions.

Figure 4a shows a typical predicted normalized footprint ($z_o f$) as a function of downwind distance (fetch) by the Lagrangian model (solid line) and measurements (circles) over a homogeneous peach orchard canopy (Leclerc et al., 2003) under near neutral condition. The measurement height, z_m, is 6 m and the surface conditions are $L \approx$ -1000 m, $u_* \approx 0.3$ m/s, $z_o \approx 0.5$ m, $h \approx 4.0$ m, and $d \approx 2.5$ m. Readers are referred to Leclerc et al. (2003) for details about the measurements. Figure 4b is the same as Figure 4a but for near neutral condition, $L \approx -200$ m and $u_* \approx 0.48$ m/s. Figures 5a and 5b are the same as Figure 4a but for unstable conditions $(z-d)/L = -0.32$ and $(z-d)/L = -0.15$, respectively. The surface conditions for Figures 4 and 5 are $z_o \approx 0.4$ to 0.54 m, $h \approx 3.1$ to 4.2 m, $d \approx 2.1$ to 2.8 m, and $u_* \approx 0.3$ to 0.4 m/s. Good agreement between measurements and predictions was found in Figures 4 and 5. As expected, under unstable atmospheric conditions the peak source location (the source with the maximum contribution to the flux measurement) is closer to the measurement location than under neutral conditions.

Also, the source area is more spread in near-neutral atmospheric stability conditions when compared to its unstable counterpart.

4.2 Model Testing over the Bare Soil Site

Before we discuss the Lagrangian model simulations, we examine the velocity and temperature profiles solved by the second-order closure model over the bare soil area first.

4.2.1 Second-Order Closure Model Calculations

Figure 6a shows typical evolution of the mean wind velocity profiles from the upwind to the downwind irrigated area where the atmospheric surface boundary conditions are $\Theta_{o1} = 313\ ^{o}K$, $\Theta_{o2} \approx 300\ ^{o}K$, $u_{*o1} = 0.4$ m/s, and $H_{o1} = 0.24\ m^{o}K/s$; here the subscript o1 and o2 denote the upwind and downwind conditions, respectively. Notice that the mean velocity profile is not changing appreciably with downwind distance. Furthermore, this minor change is due to changes in the local atmospheric stability conditions (from unstable to stable) and not due to roughness changes. Figure 6b is the same as Figure 6a but for the mean temperature profiles. Notice the dramatic change in temperature profile due to the step change in surface temperature (from hot to cool) over the bare soil. Also, in Figure 6b, the changes in temperature profiles were progressively becoming smaller and smaller with distance and the upper air layers (above 10 m from the ground) were not "sensing" the wet surface despite that the air has traveled some 90 m along the discontinuity. These simulations demonstrate that upwind air was equilibrating with the downwind surface gradually, as expected for a surface with such a small z_o.

4.2.2 Model Flux Footprint Prediction

Using the flow and the second moments computed by the closure model, we consider the footprint of water vapor flux over the bare soil area. Figure 7a shows the computed footprint as a function of downwind distance for three observation heights (1.12, 1.96 and 2.9 m, respectively), where the upwind atmospheric condition ($x < 0$) is unstable, and the downwind ($x > 0$) condition is stable. Here the fetch is 100 m (i.e., the tower is at $x = 100$ m from the boundary between irrigated and non-irrigated regions along the mean wind direction) and the atmospheric stability conditions were the same as Figure 6a. In Figure 7a, note that the sources has a maximum contribution to the flux measurement at 1.12 m is around 20 m away from the tower, and the source area expands further and further when the observation level increases. Figure 7b is the same as Figure 7a but for the neutral upwind atmospheric condition ($H_{o1} = 0.0$ m^oK/s). Comparison between Figures 7a and 7b reveals that, unlike the homogeneous case, the footprint (source area) under this in-homogeneity is only slightly influenced by atmospheric stability conditions and appears a little bit narrower if the atmospheric stability conditions become unstable.

The bare soil site experiment provides a baseline data set to test the Lagrangian model over a non-homogeneous surface since the source area for water vapor is (i) uniform, (ii) spatially well defined, and (iii) the momentum roughness change is negligible. Previous work by Hsieh et al. (1997, Figs. 8 and 9) demonstrated the need of including the non-homogeneity effects to improve the scalar flux estimation by a Lagrangian model. Here, we explicitly consider the inhomogeneity by using the mean velocity and atmospheric stability fields computed from the second-order closure model

(vis-à-vis MOST as in Hsieh et al. 1997). Figure 8 compares the water vapor flux measured by the eddy-correlation system at 1.12 m and the Lagrangian dispersion model predictions. In these runs, the atmospheric stability varied from neutral to strongly unstable conditions. Good agreement between the measurements and predictions is noted and this agreement demonstrates the usefulness of a coupled Lagrangian-Eulerian model for estimating simultaneously the scalar flux and footprint over such an irrigated bare soil site experiencing a step change in surface temperature and water vapor.

4.3 Model Testing over the Potato Site

The variations of the mean wind velocity and temperature are presented in Baldocchi and Rao (1995) and will not be repeated here given that our focus is on the latent heat flux longitudinal variations. Using the water vapor fluxes measured at 1 m downwind from the edge as a reference for the Lagrangian model, Figure 9 compares the eddy-correlation measured and Lagrangian model predicted water vapor fluxes as a function of downwind distance (fetch). As in Figure 8, the measured water vapor fluxes agreed well with model predictions.

5. Conclusion

We examined a two-dimensional Lagrangian stochastic dispersion model for predicting scalar fluxes and their footprint for planar homogeneous and inhomogeneous turbulent flows. We showed that the coupling between second-order closure modeling and Lagrangian model calculations permits explicit accounting of the effects of

inhomogeneity on footprint calculations. Using this combination, we showed that the Lagrangian model predictions of water vapor fluxes are in good agreement with field measurements over an irrigated bare soil site and an irrigated potato field. Future work will focus on extending this coupled Eulerian-Lagrangian approach to flows on complex terrain where W(x, z) becomes significant and a re-circulation zone in the mean streamlines may exist (e.g., Poggi et al., 2007).

Acknowledgment

The authors would like to thank the National Science Council, Taiwan for their support.

Appendix: Stability correction functions and Lagrangian time scale profiles

1. For unstable condition (L < 0):

$$\psi_m = -2\ln\left(\frac{1+\phi}{2}\right) - \ln\left(\frac{1+\phi^2}{2}\right) + 2\tan^{-1}(\phi) - \frac{\pi}{2} \tag{A.1}$$

$$t_L = \frac{k(z-d)u_*}{\sigma_w^2 \phi_h} \tag{A.2}$$

$$\phi = \left(1 - 16(z-d)/L\right)^{1/4} \tag{A.3}$$

$$\phi_h = 0.37\left(0.03 - 3(z-d)/L\right)^{-1/3} \tag{A.4}$$

2. For neutral and stable (L > 0) conditions:

$$\psi_m = 1 + 5(z-d)/L \tag{A.5}$$

$$t_L = \frac{k(z-d)u_*}{\sigma_w^2 \phi_h} \tag{A.6}$$

$$\phi_h = 1 + 5(z-d)/L \tag{A.7}$$

Appendix: Boundary Condition for the Second-Order Closure Model

Near the ground, the boundary values for velocity and scalars are solved by assuming that the available energy is conserved. In other words, the equation

$$LE_{o1} + H_{o1} = LE_{o2} + H_{o2} \tag{A.8}$$

is valid. With the equilibrium flux-profile relations, (A.8) can be expressed as

$$\left.\frac{\partial \Theta}{\partial z}\right|_{o2} + \frac{L}{C_p}\left.\frac{\partial Q}{\partial z}\right|_{o2} = \frac{\theta_{*o1} u_{*o1}}{kzu_{*o2}}, \tag{A.9}$$

where $\theta_* = \overline{\theta w}/u_*$. Eq. (A.9) was used to solve the boundary values.

List of Figures

Figure 1 Particle releases and their interception at a flux measurement height for inhomogeneous flow conditions and for a two-source scalar representation.

Figure 2a Comparison between measured and Lagrangian model predicted relative fluxes at 10 m above the ground as a function of downwind distance (fetch) under unstable conditions (L = -55 m, u_* = 0.4 m/s, z_o = 0.14 m, h = 0.75 m) over a homogeneous sagebrush canopy. The model A (solid line) represents the Lagrangian model prediction using the σ_u profile from (8) and the model B (dashed line) represents calculations with σ_u profile from (9).

Figure 2b Same as Figure 2a but for increased unstable conditions (L = -32 m and u_* = 0.29 m/s).

Figure 3 Same as Figure 2a but for neutral and stable (L = 100 m) conditions.

Figure 4a Comparison between measured and Lagrangian model predicted normalized footprint ($z_o f$) as a function of downwind distance (fetch) over a homogeneous peach orchard canopy under near neutral conditions. The measurement height, z_m, is 6 m and the surface conditions are L ≈ -1000 m, u_* ≈ 0.3 m/s, z_o ≈ 0.5 m, h ≈ 4.0 m, and d ≈ 2.5 m.

Figure 4b Same as Figure 4a but for near neutral condition, $L \approx -200$ m and $u_* \approx 0.48$ m/s.

Figure 5a Same as Figure 4a but for unstable conditions $(z-d)/L = -0.32$.

Figure 5b Same as Figure 4a but for unstable conditions $(z-d)/L = -0.15$.

Figure 6a Evolution of the mean wind profiles along the inhomogeneous bare soil site, where the upwind condition ($x < 0$) is unstable, and the downwind ($x > 0$) condition is stable. The boundary conditions are $\Theta_{o1} = 313\ ^oK$, $\Theta_{o2} = 300\ ^oK$, $u_{*o1} = 0.4$ m/s, and $H_{o1} = 0.24\ m\,^oK/s$. Here the subscript o1 and o2 denote the upwind and downwind conditions, respectively

Figure 6b Same as Figure 6a but for temperature.

Figure 7a Variation of the footprint as a function of measurement height and distance along the inhomogeneous surface, where the upwind condition ($x < 0$) is unstable, and the downwind ($x > 0$) condition is stable. Here the fetch is 100 m (i.e., the tower is at $x = 100$ m from the irrigated boundary along the mean wind direction) and the boundary condition is the same as Figure 6a.

Figure 7b Same as Figure 7a but the upwind atmospheric condition is near-neutral.

Figure 8 Comparison between the eddy-correlation measured and Lagrangian model predicted water vapor fluxes over the bare soil site at z = 1.12 m.

Figure 9 Comparison between eddy-correlation measured and Lagrangian model predicted water vapor fluxes as a function of downwind distance (fetch) over the potato site.

Reference

Baldocchi D.D., E. Falge, L. Gu, R. Olson, D. Hollinger, S. Running, P. Anthoni, Ch. Bernhofer, K. Davis, J. Fuentes, A. Goldstein, G. Katul, B. Law, X. Lee, Y. Malhi, T. Meyers, J.W. Munger, W. Oechel, K. Pilegaard, H.P. Schmid, R. Valentini, S. Verma, T. Vesala, K. Wilson and S. Wofsy, 2001, FLUXNET: A New Tool to Study the Temporal and Spatial Variability of Ecosystem-Scale Carbon Dioxide, Water Vapor and Energy Flux Densities, *Bull. Am. Meteorol. Soc*., 82, 2415-2435.

Baldocchi D. and S. Rao, 1995, Intra-field variability of scalar flux densities across a transition between a desert and an irrigated potato site, , *Boundary-Layer Meteor*., 76, 109-136.

Borgas, M. S., T. K. Flesch, and B. L. Sawford, 1997, Turbulent dispersion with broken reflexional symmetry, *J. Fluid Mech.*, 332, 141-156.

Brutsaert, W., 1984, Evaporation into the Atmosphere: Theory, History, and Applications, D., Reidel, Dordecht Holland, 299 pp.

Finn, D., B. Lamb, M. Leclerc, and T. W. Horst, 1996, Experimental evaluation of analytical and Lagrangian surface-layer flux footprint models, *Boundary-Layer Meteor.*, 80, 283-308.

Flesch T. K., J. D. Wilson, and E. Yee, 1995, Backward-time Lagrangian stochastic

dispersion models and their application to estimate gaseous emissions, *J. Applied Meteor.*, 34, 1320-1332.

Flesch, T. K., 1996, The footprint for flux measurements, from backward Lagrangian stochastic models, *Boundary-Layer Meteor*., 78, 399-404.

Gash, J. H. C., 1986, A note on estimating the effect of a limited fetch on micrometeorological evaporation measurements, *Boundary-Layer Meteor*., 35, 409-413.

Horst, T. W. and J. C. Weil, 1992, Footprint estimation for scalar flux measurements in the atmospheric surface layer, *Boundary-Layer Meteor*., 59, 279-296.

Horst, T. W. and J. C. Weil, 1994, How far is far enough?: The fetch requirements for micrometeorological measurement of surface fluxes, *Journal of Atmospheric and Oceanic Technology*, 11, 1018-1025.

Hsieh, C.I., G.G. Katul, and T.W. Chi, 2000, An approximate analytical model for footprint estimation of scalar fluxes in thermally stratified atmospheric flows, *Adv. Water Res.*, 23, 765-772.

Hsieh, C.-I., G. G. Katul, J. Schieldge, J. T. Sigmon, K. K. Knoerr, 1997, The Lagrangian stochastic model for fetch and latent heat flux estimation above uniform and non-uniform

terrain, *Water Resour. Res*., 33, 427-438.

Hsieh, C.I., and G.G. Katul, 1997, The dissipation methods, Taylor's hypothesis, and stability correction functions in the atmospheric surface layer, *J. Geophys. Res*., 102, 16391- 16405.

Kader, B. A. and A. M. Yaglom, 1990, Mean fields and fluctuation moments in unstable stratified turbulent boundary layers, *J. Fluid Mech.*, 212, 637-662.

Kaharabata, S. K., P. H. Schuepp, S. Ogunjemiyo, S. Shen, M. Y. Leclerc, R. L. Desjardins, and J. I. MacPherson, 1997, Footprint considerations in BOREAS, *J. Geophys. Res.*, 102, 29113-29124.

Katul, G. G. and M. B. Parlange, 1992, An atmospheric stability Penman Brutsaert potential evaporation model, *Water Resour. Res*., 28, 121-126.

Kljun N., P. Kastner-Klein, E. Fedorovich, and M. W. Rotach, 2004, Evaluation of Lagrangian footprint model using data from wind tunnel convective boundary layer, Agricultural and Forest Meteorology, 127, 189-201.

Kljun N., M. W. Rotach, and H. P. Schmid, 2002, A three-dimensional backward lagrangian footprint model for a wide range of boundary-layer stratifications, Boundary-

Layer Meteorlogy, 103, 205-226.

Kurbanmuradov O. and K. Sabelfeld, 2000, Lagrangian stochastic models for turbulent dispersion in the atmospheric boundary layer, *Boundary-Layer Meteorology*, 97, 191-218.

Leclerc, M. Y. and G. W. Thurtell, 1990, Footprint prediction of scalar fluxes using a Markovian analysis, *Boundary-Layer Meteor*., 52, 247-258.

Leclerc, M. Y., S. Shen, and B. Lamb, 1997, Observations and large-eddy simulation modeling of footprints in the lower convective boundary layer, *J. Geophys. Res.*, 102, 9323-9334.

Leclerc, M. Y., N. Meskhidze, and D. Finn, 2003, Comparison between measured tracer fluxes and footprint model predictions over a homogeneous canopy of intermediate roughness, *Agric. Forest Meteorol.*, 117, 145-158.

Luhar A. K., and K. S. Rao, 1994a, Source footprint analysis for scalar fluxes measured in the flows over an inhomogeneous surface, In Air pollution modeling and its application, edited by S.-E. Gryning and M. M. Millan, Plenum Press, New York, pp. 315-323.

Luhar A. K., and K. S. Rao, 1994b, Lagrangian stochastic dispersion model simulations

of tracer data in nocturnal flows over complex terrain, *Atmospheric Environment*, 28, 3417-3431.

Marcolla B. and A. Cescatti, 2005, Experimental analysis of flux footprint for varying stability conditions in an alpine meadow, Agricultural and Forest Meteorology, 135, 291-301.

Parlange, M. B., G. G. Katul, R. H. Cuenca, M. Levent Kavvas, D. R. Nielsen, and M. Mata, 1992, Physical Basis for a time series model of soil water content, *Water Resour. Res*., 28, 2437-2446.

Poggi, D., and G.G. Katul, 2007, The ejection-sweep cycle over gentle hills covered with bare and forested surfaces, *Boundary-Layer Meteorol*., 122, 493-515.

Rao, K. S., J. C. Wyngaard, and O. R. Cote, 1974, Local advection of momentum, heat, and moisture in micrometeorology, *Boundary-Layer Meteor*., 7, 331-348.

Reynolds, A. M., 1998a, On the formation of Lagrangian stochastic models of scalar dispersion within plant canopies, *Boundary-Layer Meteorology*, 86, 333-344.

Reynolds, A. M., 1998b, On trajectory curvature as a selection criterion for valid Lagrangian stochastic dispersion models, *Boundary-Layer Meteorology*, 88, 77-86.

Schmid H.P., 2002, Footprint modeling for vegetation atmosphere exchange studies: a review and perspective, *Agric. Forest Meteorol.*, 113, 159-183.

Sawford, B. L., 1999, Rotation of trajectories in Lagrangian stochastic models of turbulent dispersion, *Boundary-Layer Meteorology*, 93, 411-424.

Stull, R. B., 1988, An Introduction to Boundary Layer Meteorology, Kluwer Academic Publishers, MA., U.S.A., 666 pp.

Thomson, D. J., 1987, Criteria for the selection of stochastic models of particle trajectories in turbulent flows, *J. Fluid Mech.*, 180, 529-556.

Wichmann, M. and E. Schaller, 1986, On the determination of the closure parameters in higher-order closure models, *Boundary-Layer Meteor.*, 37, 323-341.

Wilson, J. D. and T. K. Flesch, 1997, Trajectory curvature as a selection criterion for valid Lagrangian stochastic models, *Boundary-Layer Meteorology*, 84, 411-426.

Inhomogeneous Condition

⇒ Wind

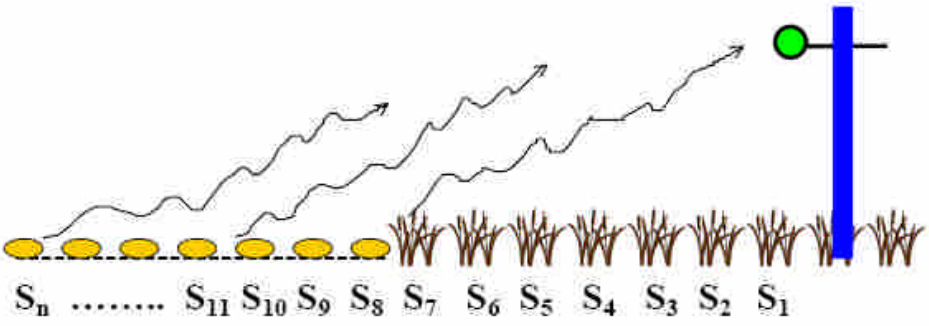

Source Area 2 **Source Area 1**

Figure 1

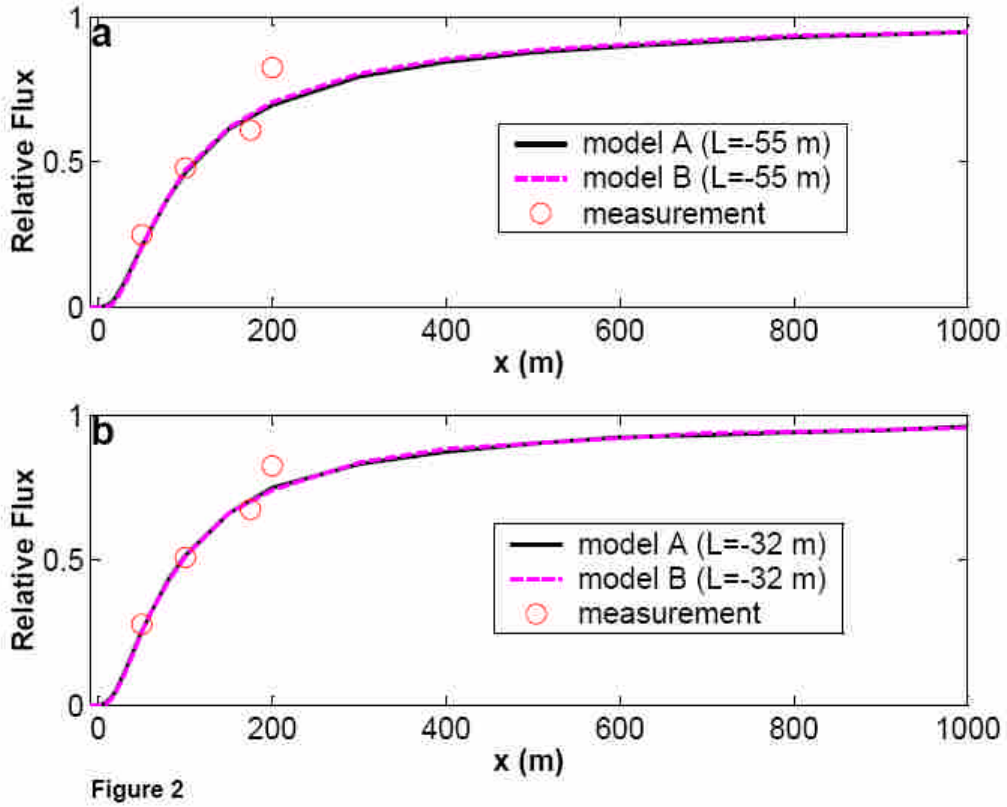
a
Relative Flux
1
0.5
0
0
200
400
600
800
1000
x (m)
model A (L=-55 m)
model B (L=-55 m)
measurement
b
Relative Flux
1
0.5
0
0
200
400
600
800
1000
x (m)
model A (L=-32 m)
model B (L=-32 m)
measurement

Figure 2

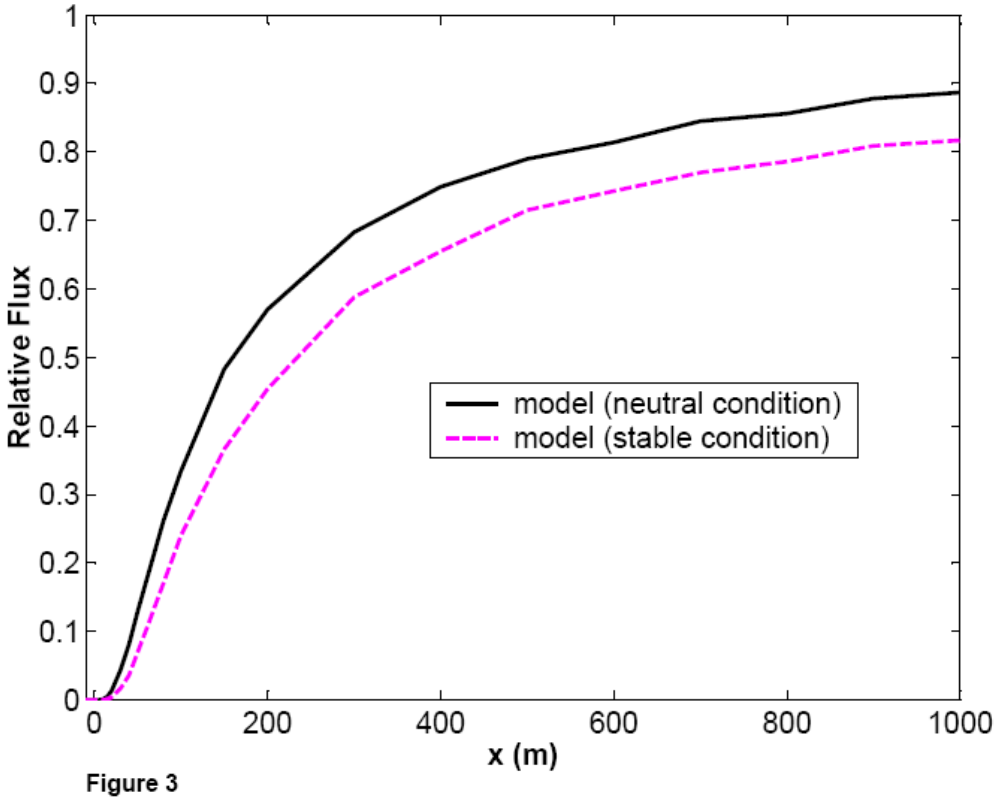
Relative Flux
x (m)
model (neutral condition)
model (stable condition)
0
0.1
0.2
0.3
0.4
0.5
0.6
0.7
0.8
0.9
1
0
200
400
600
800
1000

Figure 3

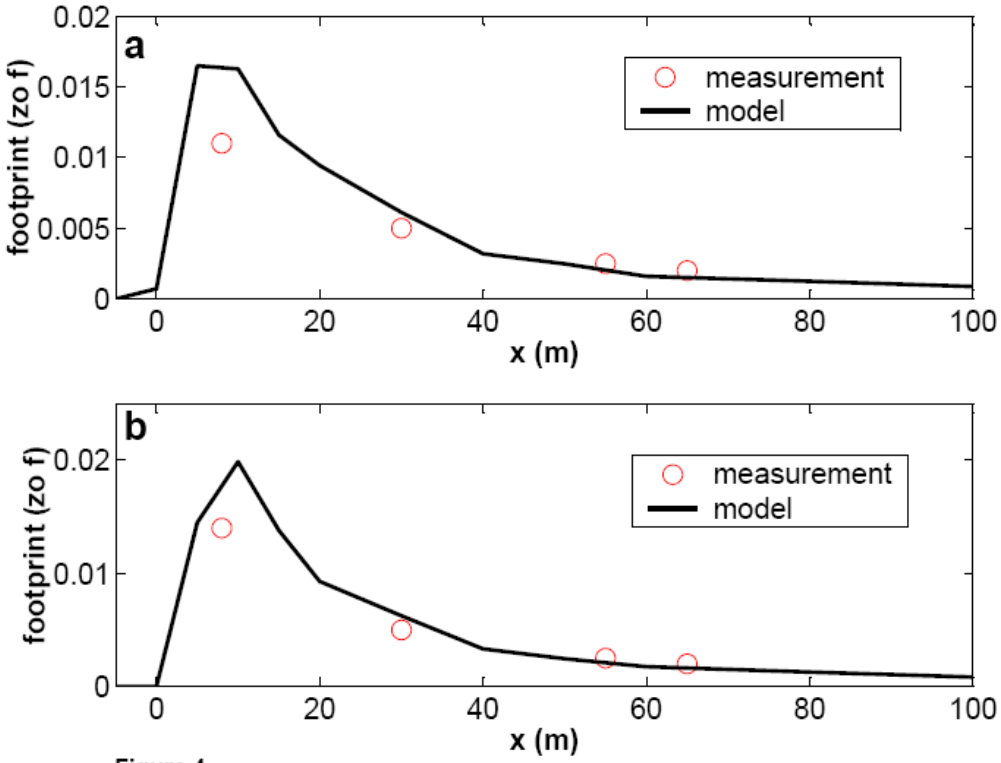
a
measurement
model
footprint (zo f)
0.02
0.015
0.01
0.005
0
0
20
40
60
80
100
x (m)
b
measurement
model
footprint (zo f)
0.02
0.01
0
0
20
40
60
80
100
x (m)

Figure 4

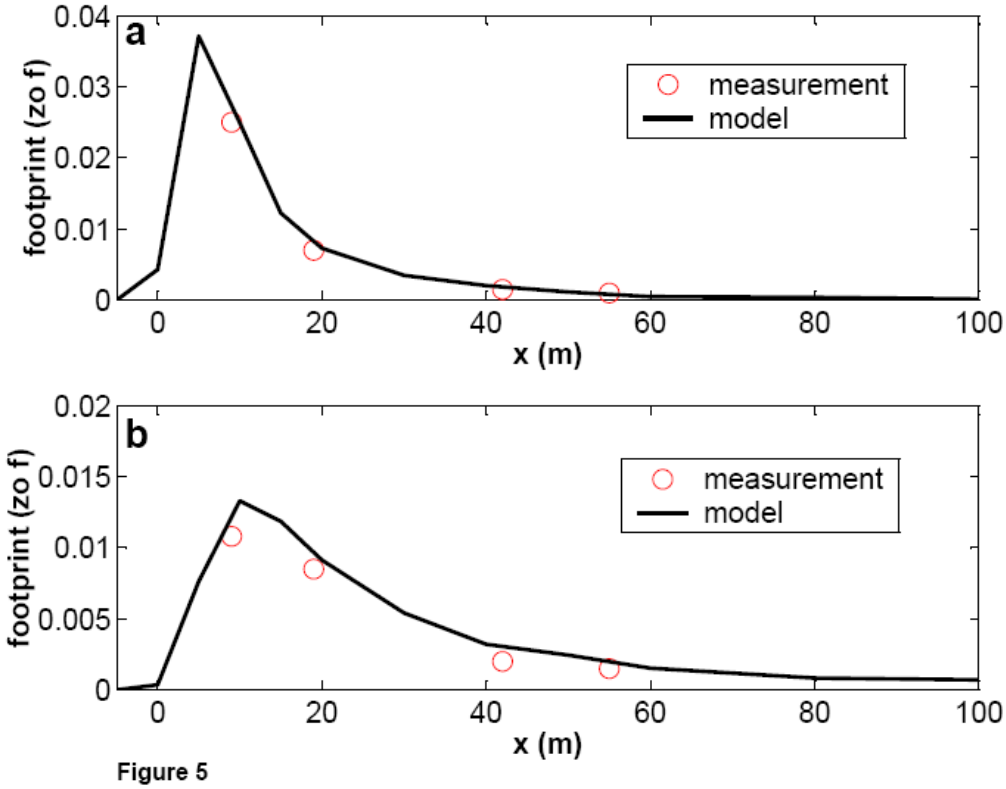
a
footprint (zo f)
0.04
0.03
0.02
0.01
0
0
20
40
60
80
100
x (m)
measurement
model
b
footprint (zo f)
0.02
0.015
0.01
0.005
0
0
20
40
60
80
100
x (m)
measurement
model

Figure 5

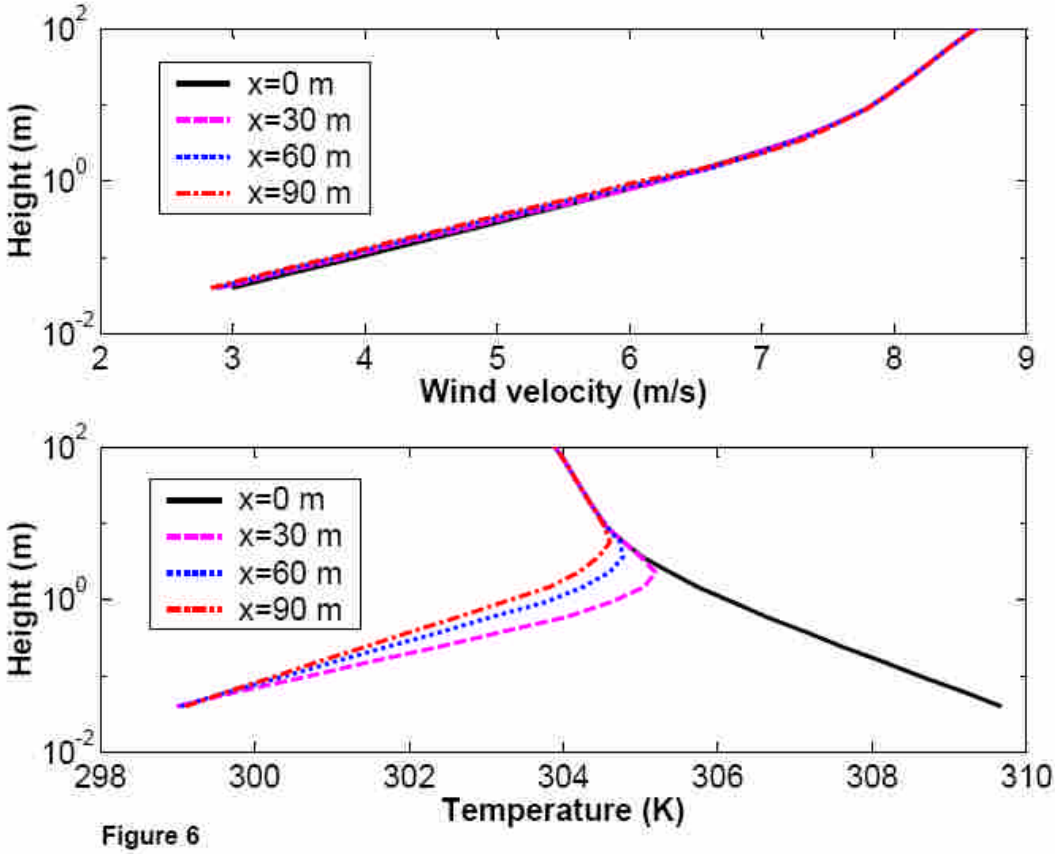
Height (m)
10^2
10^0
10^{-2}
x=0 m
x=30 m
x=60 m
x=90 m
2
3
4
5
6
7
8
9
Wind velocity (m/s)
Height (m)
10^2
10^0
10^{-2}
x=0 m
x=30 m
x=60 m
x=90 m
298
300
302
304
306
308
310
Temperature (K)

Figure 6

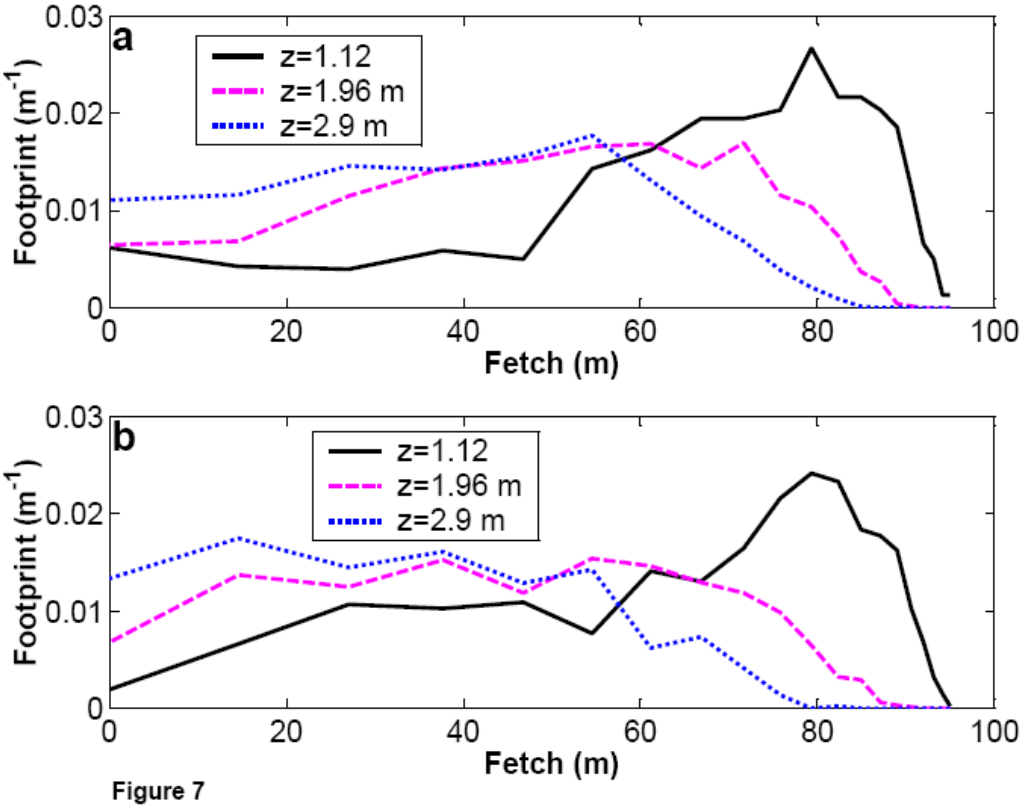
a
z=1.12
z=1.96 m
z=2.9 m
Footprint (m-1)
0.03
0.02
0.01
0
0
20
40
60
80
100
Fetch (m)
b
z=1.12
z=1.96 m
z=2.9 m
Footprint (m-1)
0.03
0.02
0.01
0
0
20
40
60
80
100
Fetch (m)

Figure 7

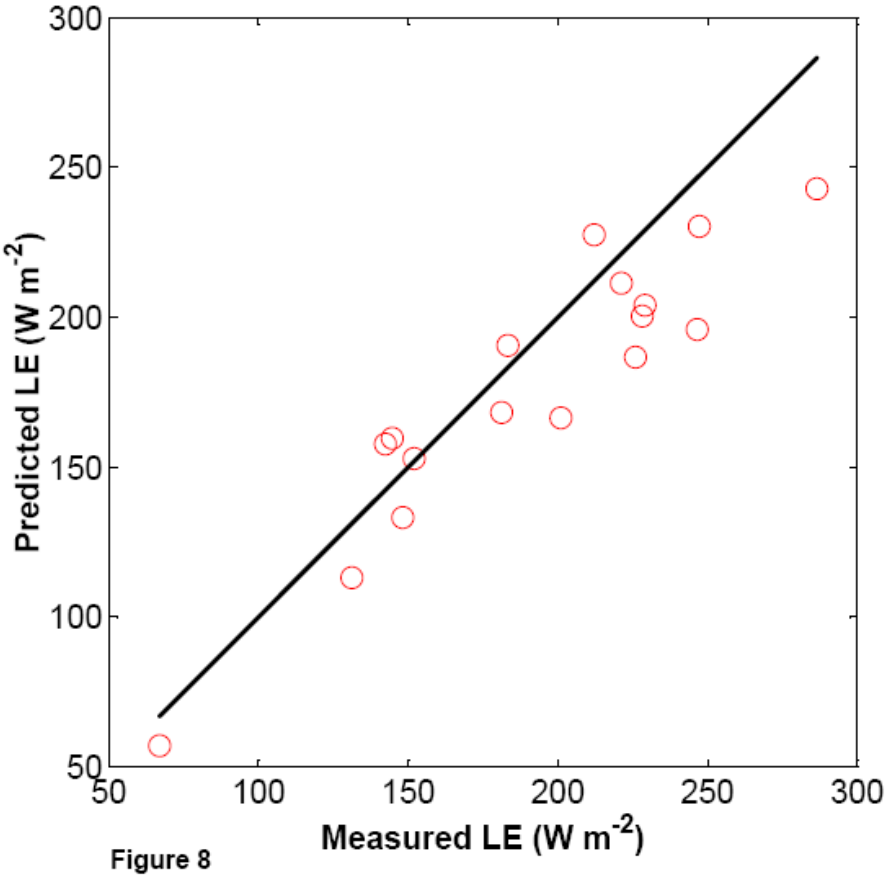
300
250
200
150
100
50
50
100
150
200
250
300
Predicted LE (W m-2)
Measured LE (W m-2)

Figure 8

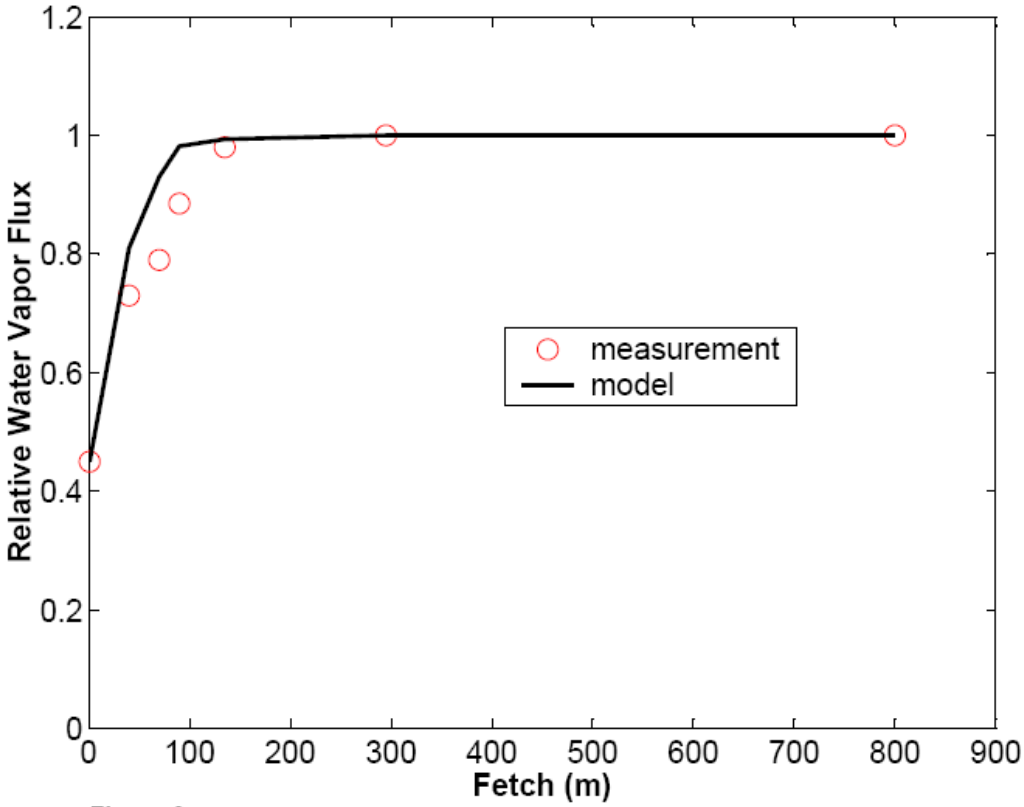
1.2
1
0.8
0.6
0.4
0.2
0
0
100
200
300
400
500
600
700
800
900
Relative Water Vapor Flux
Fetch (m)
measurement
model

Figure 9